

Characterization of Heterogeneous Nickel Sites in CO Dehydrogenases from *Clostridium thermoaceticum* and *Rhodospirillum rubrum* by Nickel L-Edge X-ray Spectroscopy

C. Y. Ralston,^{†,‡} Hongxin Wang,[‡] S. W. Ragsdale,[§] M. Kumar,[§] N. J. Spangler,^{||} P. W. Ludden,^{||} W. Gu,[‡] R. M. Jones,[⊥] D. S. Patil,[⊥] and S. P. Cramer^{*,‡,⊥}

Contribution from the Department of Applied Science, University of California, Davis, California 95616, Department of Biochemistry, University of Nebraska, Lincoln, Nebraska 68583, Department of Biochemistry, University of Wisconsin, Madison, Wisconsin 53706, and Lawrence Berkeley National Laboratory, Berkeley, California 94720

Received March 16, 2000

Abstract: Carbon monoxide dehydrogenase from *Clostridium thermoaceticum* (Ct-CODH) is a nickel-containing enzyme that catalyzes acetyl-CoA synthesis and CO oxidation at two separate Ni sites, the A-cluster and C-cluster, respectively. Carbon monoxide dehydrogenase from *Rhodospirillum rubrum* (Rr-CODH) contains only a C-type cluster and catalyzes only CO oxidation. We have used L-edge X-ray absorption spectroscopy to study the Ni electronic structure of these two enzymes. The spectra indicate that most of the Ni in as-isolated Ct-CODH is low-spin Ni(II). Upon CO treatment, a fraction of the nickel is converted either to high-spin Ni(II) and/or to Ni(I). Ni in dithionite-reduced Rr-CODH also exhibits a clear low spin Ni(II) component, again mixed with either high-spin Ni(II) or Ni(I). The spectrum of Rr-CODH shifts to higher energy upon indigo carmine oxidation, suggesting either that most of the high-spin Ni(II) is converted to low-spin Ni(II) and/or that some Ni is oxidized between these two forms. These results are discussed and compared with recent L-edge spectra for the Ni site in hydrogenase.

Introduction

The Wood-Ljungdahl pathway describes the biochemical steps involved in anaerobic fixation of carbon dioxide and synthesis of acetate.^{1,2} Apart from their biochemical and environmental significance, these reactions are analogous to important industrial processes.³ In *Clostridium thermoaceticum*, CO oxidation and acetyl-CoA synthesis are catalyzed by carbon monoxide dehydrogenase (Ct-CODH), a 310 kDa ($\alpha\beta$)₂ tetramer.^{4,5} In the photosynthetic bacterium *Rhodospirillum rubrum*, there is a related enzyme (Rr-CODH)—a monomer that catalyzes only the first reaction.



Ct-CODH catalysis involves two physically distinct sites,^{4–8} the “C-cluster” and “A-cluster”, which both contain Ni and

Fe.^{9–13} Each $\alpha\beta$ dimer contains 2 Ni and 11–14 Fe^{7,14} and presumably incorporates one A-cluster and one C-cluster. There is also a conventional [Fe₄S₄]^{2+/1+} “B-cluster”,¹⁵ which transfers electrons between the C-cluster and external redox agents.⁵

The A-cluster contains the acetyl-CoA synthesis site and is EPR-silent in the as-isolated “A_{ox}” form. It generates a “Ni–Fe–C” EPR signal when Ct-CODH is treated with CO^{16,17} to yield “A_{red}-CO”. Mössbauer and ENDOR studies suggest a structure involving Ni bridged to an Fe₄S₄ cluster.^{8,11,18,19} The CO oxidation site C-cluster has been proposed to have a similar structure.¹³ This cluster occurs in two EPR-active forms, “C_{red1}” and “C_{red2}”, as well as an EPR-silent “C_{ox}” form, along with other states.

Rr-CODH is a 66.9-kDa protein containing 1 Ni and 7–8 Fe,²⁰ with an associated 22-kDa subunit containing an additional

[†] Current address: Department of Biophysics and Physiology, Albert Einstein College of Medicine, Yeshiva University, The Bronx, NY 10461.

[‡] University of California.

[§] University of Nebraska.

^{||} University of Wisconsin.

[⊥] Lawrence Berkeley National Laboratory.

- (1) Ferry, J. G. *Annu. Rev. Microbiol.* **1995**, *49*, 305–333.
- (2) Ragsdale, S. W.; Kumar, M. *Chem. Rev.* **1996**, *96*, 2515–2539.
- (3) Qiu, D.; Kumar, M.; Ragsdale, S. W.; Spiro, T. G. *Science* **1994**, *264*, 817–819.
- (4) Raybuck, S. A.; Bastian, N. R.; Orme-Johnson, W. H.; Walsh, C. T. *Biochemistry* **1988**, *27*, 7698–7702.
- (5) Kumar, M.; Lu, W.-P.; Liu, L. F.; Ragsdale, S. W. *J. Am. Chem. Soc.* **1993**, *115*, 11646–11647.
- (6) Shin, W.; Lindahl, P. A. *J. Am. Chem. Soc.* **1992**, *114*, 9718–9719.
- (7) Xia, J. Q.; Sinclair, J. F.; Baldwin, T. O.; Lindahl, P. A. *Biochemistry* **1996**, *35*, 1965–1971.
- (8) Xia, J.; Lindahl, P. A. *J. Am. Chem. Soc.* **1996**, *118*, 483–484.

(9) Ragsdale, S. W.; Wood, H. G.; Antholine, W. E. *Proc. Natl. Acad. Sci. U.S.A.* **1985**, *82*, 6811–6814.

(10) Ragsdale, S. W.; Ljungdahl, L. G.; DerVartanian, D. V. *Biochem. Biophys. Res. Commun.* **1983**, *115*, 658–665.

(11) Lindahl, P. A.; Ragsdale, S. W.; Münck, E. *J. Biol. Chem.* **1990**, *265*, 3880–3888.

(12) Ensign, S. A.; Campbell, M. J.; Ludden, P. W. *Biochemistry* **1990**, *29*, 2162–2168.

(13) Hu, Z. G.; Spangler, N. J.; Anderson, M. E.; Xia, J. Q.; Ludden, P. W.; Lindahl, P. A.; Münck, E. *J. Am. Chem. Soc.* **1996**, *118*, 830–845.

(14) Ragsdale, S. W.; Clark, J. E.; Ljungdahl, L. G.; Lundie, L. L.; Drake, H. L. *J. Biol. Chem.* **1983**, *258*, 2364–2369.

(15) Lindahl, P. A.; Münck, E.; Ragsdale, S. W. *J. Biol. Chem.* **1990**, *265*, 3873–3879.

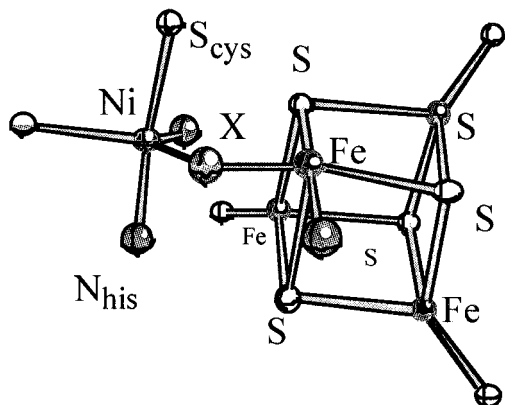
(16) Ragsdale, S. W.; Ljungdahl, L. G.; der Vartanian, D. V. *Biochem. Biophys. Res. Commun.* **1982**, *108*, 658–663.

(17) Gorst, C. M.; Ragsdale, S. W. *J. Biol. Chem.* **1991**, *266*, 20687–20693.

(18) Fan, C. L.; Gorst, C. M.; Ragsdale, S. W.; Hoffman, B. M. *Biochemistry* **1991**, *30*, 431–435.

(19) Xia, J. Q.; Hu, Z. G.; Popescu, C. V.; Lindahl, P. A.; Münck, E. *J. Am. Chem. Soc.* **1997**, *119*, 8301–8312.

Scheme 1. Essential Features of the Ni-X-Fe₄S₄ Structures that Has Been Proposed for Both the A-Cluster²³ and the C_{Red1} Form of the C-Cluster.^{13,a}



^a The number and geometry of the Ni ligands is probably different between A and C clusters.

Fe-S cluster.²¹ Genetic characterization of the two enzymes has shown that Rr-CODH is 67% similar to the β subunit of Ct-CODH.²² It contains an Fe₄S₄ cluster and a catalytic center analogous respectively to the B-cluster and C-cluster of Ct-CODH.¹³ EXAFS analysis of Rr-CODH provided evidence for both S and N/O ligation to the Ni.²⁴ The Ct-CODH Ni EXAFS is also dominated by Ni-S interactions,²⁵ but weaker Ni-N/O components may be present.²⁶ Interpretation of the Ni EXAFS of native Ct-CODH, however, is complicated by the heterogeneity of the samples—signals from different Ni sites are averaged together in the spectra, and the ligation of the individual sites cannot be determined. To simplify the analysis, Xia and co-workers examined the EXAFS of the α subunit of Ct-CODH, obtained by gel electrophoresis of SDS-dissociated protein.²⁷ They concluded that the Ni site has a distorted square planar Ni with 2S at 2.19 Å and 2N,O donor ligands at 1.89 Å. From the differences between the α subunit and the intact CODH spectra, they inferred that C-cluster Ni is most likely in a distorted five-coordinate or tetrahedral geometry. In the above studies, the Ni-Fe distances and the nature of possible Ni-Fe bridging interactions remained ambiguous.

There is little direct information about the electronic structure of the Ni ions in the various forms of the A- and C-clusters. The “Ni-Fe-C” EPR signal exhibits ⁶¹Ni hyperfine broadening,^{15,16} as does the “pseudo-Ni-Fe-C” signal from the α subunit.^{8,19} In a model developed by Münck and co-workers, this is explained by a Ni(I) species exchange-coupled with one Fe site of a [Fe₄S₄]²⁺ cluster through a bridging ligand X.¹⁹ They also proposed a Ni(II) species for the oxidized A-cluster, based on the absence of an EPR signal in this form. For the “C_{Red1}” form of the C-cluster, which lacks ⁶¹Ni hyperfine

coupling, the same group proposed a high-spin $S = 1$ Ni(II) weakly coupled to a $S = 1/2$ [Fe₄S₄]¹⁺ cluster.¹³ However, they could not rule out a model with high-spin or low-spin Ni(II) electronically isolated from the [Fe₄S₄]¹⁺ cluster. Finally, Anderson and Lindahl have argued that the “C_{Red2}” form of the C-cluster contains Ni(I) and a [Fe₄S₄]¹⁺ cluster. They propose that the Ni(I) is spin-coupled to the reduced form of a redox active ligand L_{red}.²⁸

L-edge X-ray absorption spectroscopy (XAS) has been extensively used as a probe of electronic structure in transition metal compounds,²⁹ but it is still a relatively new technique for characterization of metalloprotein electronic structure.^{30,31} For first transition metal ions, L-edge spectra involve transitions from 2p⁶3d^N to 2p⁵3d^{N+1} configurations. The spectral intensities are sensitive to the number of d-holes available.³² The spectral energies and relative intensities are sensitive to the oxidation and spin state changes of the absorbing element.²⁹ In favorable cases the strength and symmetry of the ligand field can be inferred.^{33,34}

We have previously used L-edge XAS to probe Fe^{35–37} and Cu^{38–40} proteins, as well as the Ni sites in Ni-substituted rubredoxin³⁴ and in *Pyrococcus furiosus* hydrogenase.^{41,42} We report here the L-edge XAS spectrum of the native and CO-treated forms of Ct-CODH, and the dithionite-reduced and indigo carmine oxidized forms of Rr-CODH. In a companion paper, we examine the Ni in a variety of hydrogenase samples.⁴³ The results provide information about the Ni oxidation state and spin states in these enzymes which has been unavailable by other techniques.

Experimental Procedures

Preparation of Protein Samples. *R. rubrum* cultures were grown and CODH was purified according to published methods.^{44,45} Rr-CODH

(20) Bonam, D.; Ludden, P. W. *J. Biol. Chem.* **1987**, *262*, 2980–2987.

(21) Ensign, S. A.; Ludden, P. W. *J. Biol. Chem.* **1991**, *266*, 18395–18403.

(22) Kerby, R. L.; Hong, S. S.; Ensign, S. A.; Coppoc, L. J.; Ludden, P. W.; Roberts, G. P. *J. Bacteriol.* **1992**, *174*, 5284–5294.

(23) Tucci, G. C.; Holm, R. H. *J. Am. Chem. Soc.* **1995**, *117*, 6489–6496.

(24) Tan, G. O.; Ensign, S. A.; Ciurli, S.; Scott, M. J.; Hedman, B.; Holm, R. H.; Ludden, P. W.; Korsun, Z. R.; Stephens, P. J.; Hodgson, K. O. *Proc. Natl. Acad. Sci. U.S.A.* **1992**, *89*, 4427–4431.

(25) Bastian, N. R.; Diekert, G.; Niederhoffer, E. C.; Teo, B.-K.; Walsh, C. T.; Orme-Johnson, W. H. *J. Am. Chem. Soc.* **1988**, *110*, 5581–5582.

(26) Cramer, S. P.; Eidsness, M. K.; Pan, W.-H.; Morton, T. A.; Ragsdale, S. W.; DerVartanian, D. V.; Ljungdahl, L. G.; Scott, R. A. *Inorg. Chem.* **1987**, *26*, 2477–2479.

(27) Xia, J. Q.; Dong, J.; Wang, S. K.; Scott, R. A.; Lindahl, P. A. *J. Am. Chem. Soc.* **1995**, *117*, 7065–7070.

(28) Anderson, M. E.; Lindahl, P. A. *Biochemistry* **1996**, *35*, 8371–8380.

(29) deGroot, F. M. F. *J. Electron Spectrosc. Relat. Phenom.* **1994**, *67*, 529–622.

(30) deGroot, F. M. F.; Fuggle, J. C.; Thole, B. T.; Sawatzky, G. A. *Phys. Rev. B* **1990**, *42*, 5459–5468.

(31) Cramer, S. P.; Wang, H.; Bryant, C.; Legros, M.; Horne, C.; Patel, D.; Ralston, C.; Wang, X. In *Spectroscopic Methods in Bioinorganic Chemistry*; Solomon, E. I., Hodgson, K. O., Eds.; American Chemical Society: Washington, DC, 1998.

(32) Wang, H.; Ge, P.; Riordan, C. G.; Brooker, S.; Woomer, C. G.; Collins, T.; Mahalingam, B.; Melendres, C.; Graudejus, O. *J. Phys. Chem. B* **1998**, *102*, 8343–8346.

(33) Cramer, S. P.; Degroot, F. M. F.; Ma, Y.; Chen, C. T.; Sette, F.; Kipke, C. A.; Eichhorn, D. M.; Chan, M. K.; Armstrong, W. H.; Libby, E.; Christou, G.; Brooker, S.; Mckee, V.; Mullins, O. C.; Fuggle, J. C. *J. Am. Chem. Soc.* **1991**, *113*, 7937–7940.

(34) van Elp, J.; Peng, G.; Searle, B. G.; Mitra-Kirtley, S.; Huang, Y. H.; Johnson, M. K.; Zhou, Z. H.; Adams, M. W. W.; Maroney, M. J.; Cramer, S. P. *J. Am. Chem. Soc.* **1994**, *116*, 1918–1923.

(35) George, S. J.; Vanelp, J.; Chen, J.; Ma, Y.; Chen, C. T.; Park, J. B.; Adams, M. W. W.; Searle, B. G.; Degroot, F. M. F.; Fuggle, J. C.; Cramer, S. P. *J. Am. Chem. Soc.* **1992**, *114*, 4426–4427.

(36) van Elp, J.; George, S. J.; Chen, J.; Peng, G.; Chen, C. T.; Tjeng, L. H.; Meigs, G.; Lin, H. J.; Zhou, Z. H.; Adams, M. W. W.; Searle, B. G.; Cramer, S. P. *Proc. Natl. Acad. Sci. U.S.A.* **1993**, *90*, 9664–9667.

(37) Wang, H. X.; Peng, G.; Miller, L. M.; Scheuring, E. M.; George, S. J.; Chance, M. R.; Cramer, S. P. *J. Am. Chem. Soc.* **1997**, *119*, 4921–4928.

(38) George, S. J.; Lowery, M. D.; Solomon, E. I.; Cramer, S. P. *J. Am. Chem. Soc.* **1993**, *115*, 2968–2969.

(39) Christiansen, J.; Peng, G. A. T.; Young, A. T.; LaCroix, L. B.; Solomon, E. I.; Cramer, S. P. *Inorg. Chem. Acta* **1996**, *118*, 229–232.

(40) Wang, H. C.; Bryant, C.; LaCroix, L. B.; Randall, D. W.; Solomon, E. I.; LeGros, M. *J. Phys. Chem. B* **1998**, *102*, 8347–8349.

(41) van Elp, J.; Peng, G.; Zhou, Z. H.; Adams, M. W. W.; Baidya, N.; Mascharak, P. K.; Cramer, S. P. *Inorg. Chem.* **1995**, *34*, 2501–2504.

(42) Cramer, S. P.; Peng, G.; Christiansen, J.; Chen, J.; van Elp, J.; George, S. J.; Young, A. T. *J. Electron Spectrosc. Relat. Phenom.* **1996**, *78*, 225–229.

(43) Wang, H. *J. Am. Chem. Soc.* **2000**, *122*, 10544–10552.

samples were prepared in an anaerobic box containing less than 1 ppm oxygen (Vacuum/Atmospheres Dri-Lab glovebox, model HE-493). Rr-CODH in 100 mM MOPS (3-(*N*-morpholino)propanesulfonic acid) at pH 7.5 containing 400 mM NaCl and ~ 2 mM dithionite was stripped of NaCl and dithionite by passage through a Sephadex G-25 column equilibrated in 100 mM MOPS, pH 7.5. Rr-CODH was oxidized by adding indigo carmine (~ 3 mM), and indigo carmine was removed as previously described.¹² This partially oxidized sample should correspond to $[B_{ox}:C_{ox}:C_{red1}]$ Rr-CODH in the nomenclature of Hu *et al.*¹³ In the current paper, we refer to this sample as “indigo carmine oxidized Rr-CODH”. The “dithionite-reduced Rr-CODH” sample was prepared by adding dithionite to the desalted enzyme to a final concentration of 2 mM. This sample should correspond to fully reduced or $[B_{red}:C_{red2}:C_{S=3/2}]$ Rr-CODH in the nomenclature of Hu *et al.*¹³ The concentration of the Rr-CODH sample used to prepare films was 29 mg mL⁻¹. The protein concentration was determined by the bicinchoninic acid colorimetric method using bovine serum albumin (grade A, Sigma) as standard.⁴⁶ CO-oxidation activity was determined by the CO-dependent methylviologen reduction assay.⁴⁴ One unit of activity equals 1 μ m CO-oxidized per minute.

Ct-CODH was purified essentially as previously described,^{7,14} using *C. thermoacetium* strain ATCC 39073 grown on glucose at 55 °C.⁴⁷ The specific activity of purified Ct-CODH for the first round of experiments was 300–450 units mg⁻¹ (1 unit = 1 μ mol CO oxidized min⁻¹) at 55 °C in the standard assay using 50 mM Tris-HCl, pH 7.6, with 10 mM methylviologen as electron acceptor. The samples used in the second round of experiments had a CO oxidation specific activity of 500 units/mg. The specific activity of the Ct-CODH in the isotope exchange reaction between CO and $[1-^{14}C]$ acetyl-CoA was 183 nmol min⁻¹ mg⁻¹ at 55 °C using 0.49 mM acetyl-CoA and 1 mM CO in 100 mM Tris-maleate, pH 5.5. The samples used in the second round of experiments had an exchange specific activity of 0.290 unit/mg. The concentration of the Ct-CODH sample used for the preparation of L-edge samples was 57–61 mg mL⁻¹ (0.38–0.4 mM) for the first round and 0.1 mM for the second round.

Enzyme Film Preparation and Sample Transfer. Method 1. The CODH samples were initially prepared as partially dehydrated films by placing a drop of protein sample (~ 10 μ L) on a silicon wafer and allowing the enzyme to dry under a N₂ atmosphere in an anaerobic chamber. The back of the silicon wafer was then glued to a threaded gold-plated copper mount for attachment to the coldfinger. In the case of CO-treated Ct-CODH, a CO atmosphere was maintained during the drying process using a desiccator jar filled with CO. All samples were transferred anaerobically to the X-ray spectroscopy vacuum chamber, using a load-lock and magnetic transfer arm, where they were mounted onto a gold-plated coldfinger. During this transfer process, the time interval over which samples were under vacuum but not frozen was approximately 25 min. The coldfinger temperature was maintained at 20–30 K throughout the data collection.

Enzyme Film Preparation and Sample Transfer. Method 2. After the first round of experiments, reasonable concerns were expressed by referees and others about possible changes in resting or CO-treated Ct-CODH enzyme, both during film preparation and while being transferred through the load-lock. We therefore devised a method for keeping the enzyme under the appropriate atmosphere until reaching ~ 20 K on the chamber coldfinger. In these experiments, the previous silicon support was replaced by a 1 mm thick \times 5 mm diameter sapphire plate. Control or CO-treated CODH film samples were prepared by placing 20 μ L of the appropriate enzyme solution on this plate. This sample was then allowed to dry either in the glovebox or in a small jar under a pure CO atmosphere. The plate was mounted on a copper support and sealed with a cap under a N₂ or CO atmosphere. The sealed cell was transferred through a loadlock into the vacuum chamber and

threaded onto the 20 K coldfinger. After ~ 30 min, the cap was unthreaded and the X-ray experiments commenced.

Checks of Protein Sample Integrity. To ensure that samples were able to withstand the film creation process, assays were performed on material before and after drying, both in parallel experiments and in some cases on the same samples used for X-ray spectroscopy. In the case of Rr-CODH, 10- μ L aliquots of a sample with an initial activity of 3620 ± 220 units/mg were dried on microscope slide cover slips under conditions analogous to X-ray sample creation. Samples were dried for 1, 2, 3, and 4 h, dissolved in 100 mM MOPS, pH 7.5, and assayed. Activities of 3750 ± 235 , 3640 ± 350 , 3650 ± 130 , and 3720 ± 120 units/mg were measured for the 1-, 2-, 3-, and 4-h samples, respectively. In addition to recovering 100% of the original activity, 100% of the dried protein was recovered in solution as well. The Rr-CODH samples used for L-edge experiments initially had a specific activity of 2670 units mg⁻¹.

For the native Ct-CODH samples, the specific activity of one sample for CO oxidation before drying on Si was 297 units/mg. In a laboratory test, after drying the CODH on Si, then scraping off a fraction and dissolving in 50 mM Tris/HCl at pH 7.6, the CO oxidation specific activity was 276 units/mg. Thus, the drying procedure only slightly diminishes enzyme activity. For one sample from this batch, after L-edge and EPR analyses, the specific activity for CO oxidation was 185 units/mg. Some of the damage may occur after warming the X-ray exposed sample, when the free radicals generated by the X-ray beam become mobile. For one CO-treated sample, the specific activity for CO oxidation, before CO treatment, was 437 units/mg. After CO treatment but before L-edge analysis, the specific activity for CO oxidation was 406 units/mg. After L-edge analysis, the specific activity measured for CO oxidation was 238 units/mg.

Preparation of Model Compounds. The Ni model compounds used for this investigation were synthesized according to published procedures, as referenced in the companion paper.⁴³

L-Edge Measurements. The first round of protein Ni L-edge spectra were recorded at beamline 10-1 at the Stanford Synchrotron Radiation Laboratory (SSRL) and at beamline U4-B⁴⁸ at the National Synchrotron Light Source (NSLS). The spectrometer energy resolutions used for protein samples and for Ni model compound spectra were 350 and 270 meV, respectively. The more recent “capped-cell” protein spectra were recorded on SSRL beamline 8-2 with ~ 1.5 -eV resolution.⁴⁹ During all X-ray measurements, the sample chamber was maintained at less than 5×10^{-9} Torr using a helium cryopump.

Model compound spectra were measured in total electron yield mode with a channeltron electron multiplier as detector.⁵⁰ The protein spectra were recorded using fluorescence detection with a windowless 13-element germanium detector.⁵¹ In all cases, the incident beam intensity was measured by using the total electron yield from a gold-coated grid placed between the sample and the monochromator.

The L-edge spectra were calibrated by using the total electron yield spectrum of NiF₂ or NiO, which have absorption maxima at 852.7 and 853.2 eV,⁵² respectively. Each protein spectrum presented represents the sum of about 40 20-min scans. Calibration spectra were run hourly during protein scans to monitor beam stability and resolution. To minimize radiation damage, the position of the X-ray beam on the sample was moved every few scans. No evidence was observed for changes over time in the spectra. All of the reported changes in protein spectra were reproduced on 2–4 different occasions at different beamlines with separate batches of samples.

L-Edge XAS Data Analysis. The background from absorption by oxygen and other elements was approximated by a polynomial fit to the low-energy region before the L₃ edge and to the high-energy region beyond the L₂ edge. This polynomial baseline was then subtracted from

(44) Bonam, D.; McKenna, M. C.; Stephens, P. J.; Ludden, P. W. *Proc. Natl. Acad. Sci. U.S.A.* **1988**, *85*, 31–35.

(45) Ensign, S. A.; Bonam, D.; Ludden, P. W. *Biochemistry* **1989**, *28*, 4968–4973.

(46) Smith, M. R.; Lequerica, J. L.; Hart, M. R. *J. Bacteriol.* **1985**, *162*, 67–71.

(47) Andreesen, J. R.; Schaupp, A.; Neurater, C.; Brown, A.; Ljungdahl, L. G. *J. Bacteriol.* **1973**, *114*, 743–751.

(48) Chen, C. T.; Sette, F. *Rev. Sci. Instrum.* **1989**, *60*, 1616–1621.

(49) Tirsell, K. G.; Karpenko, V. P. *Nucl. Inst. Methods A* **1990**, *291*, 511–517.

(50) Stöhr, J. *NEXAFS Spectroscopy*; Springer-Verlag: New York, 1992.

(51) Cramer, S. P.; Chen, J.; George, S. J.; van Elp, J.; Moore, J.; Tench, O.; Colaresi, J.; Yocum, M.; Mullins, O. C.; Chen, C. T. *Nucl. Inst. Methods A* **1992**, *319*, 285–289.

(52) van der Laan, G.; Zaanen, J.; Sawatzky, G. A.; Karnatak, R.; Esteva, J.-M. *Phys. Rev. B* **1986**, *33*, 4253–4263.

the raw spectrum. The branching ratio was calculated by integrating the L_3 peak (850–856 eV) and the L_2 peak (868–874 eV) and calculating the area ratio $I(L_3)/[I(L_2) + I(L_3)]$. The L_3 centroid was calculated by integration over the energy range 850–856 eV. Errors of ± 0.1 eV in L_3 centroid position and ± 0.02 in branching ratio were estimated by calculating these parameters using various ranges of integration and by comparing results from two separate runs of the same samples.

Results

Model Compound Correlations. Computer simulations of L-edge multiplet structure are commonly used to derive information about the metal oxidation state and ligand field.²⁹ Calculated spectra have proven useful in previous studies of Ni,^{34,41} Mn,^{33,53} and Fe complexes⁵⁴ and Fe proteins.³⁵ However, there is no observable multiplet structure in the CODH L-edges, and other characteristics of the spectra must be exploited. One useful property is the L_3 centroid position, since L-edges generally shift to higher energy as the metal becomes more oxidized. A second diagnostic involves the ratio of L_3 intensity to overall intensity, $I(L_3)/[I(L_2) + I(L_3)]$, known as the “branching ratio”.²⁹ As shown by Thole and van der Laan,⁵⁵ the branching ratio for high-spin complexes is higher than for low-spin complexes, and it can therefore be used as a diagnostic of the metal spin state. A final useful property, which results from an X-ray “sum rule”,⁵⁶ is the integrated intensity of the $2p \rightarrow 3d$ transitions normalized to the continuum intensity. Since d^8 Ni(II) has approximately twice the number of d-vacancies as d^9 Ni(I), for a given amount of Ni, the integrated area under the Ni(II) L-edge features will be approximately twice the integrated area of a Ni(I) complex.³²

We examined the branching ratio and L_3 centroid position for a number of Ni compounds in different spin states and oxidation states. Many of the individual spectra are reported in the companion paper to this work.⁴³ In the spirit of the Peisach and Blumberg EPR “truth diagrams”,⁵⁷ we created a two-dimensional diagram mapping the above quantities for different types of Ni complexes. As illustrated in Figure 1, the combination of branching ratio and L_3 centroid allows the segregation of Ni spectra into different regions for Ni(I), high-spin Ni(II), low-spin Ni(II), Ni(III), and Ni(IV).

The L_3 centroid position can be used to distinguish Ni(I) and Ni(II). For the compounds in our database, the average centroid positions differ by nearly 1 eV—852.55 eV for Ni(I), 853.4 eV for high spin Ni(II), and 853.5 eV for low spin Ni(II) on our calibration scale. The L_3 centroid position turns out to be a more useful indicator than the L_3 peak position. For example, the L_3 absorption maxima of several high spin Ni(II) compounds are within 0.2 eV of those for Ni(I) compounds, making it difficult to distinguish these two species using the peak position. However, high spin Ni(II) spectra have additional higher energy features that shift the centroid of the absorption in that direction. Of course, when presented with the spectra of mixtures, it becomes hard to define the centroids of the individual components, and this limits our ability to distinguish between Ni(I) and high-spin Ni(II) in some of the protein spectra.

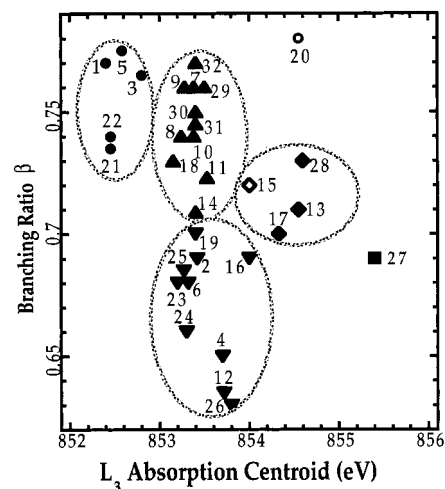


Figure 1. Two-dimensional correlation of branching ratio vs L_3 centroid position for a set of Ni model compounds with different oxidation state and spin states. Key: Ni(I) complexes—filled circles; low-spin Ni(II) complexes—inverted triangles; high-spin Ni(II) complexes—upright triangles; low-spin Ni(III) complexes—black diamonds; high-spin Ni(III)—open circle; Ni(IV)—square. Identities of compounds are included as supporting information. Ellipses are drawn only to guide the eye.

High-spin and low-spin Ni(II) often have similar centroid positions (Figure 1). In this case, these two types of Ni can usually be distinguished by the branching ratio. The experimental values for high-spin complexes ranged from 0.71 to 0.76, with an average of 0.74, while low-spin Ni(II) complexes had branching ratios ranging from 0.63 to 0.70, with an average of 0.67.

The most ionic Ni(III) complex in our sample set was K_3NiF_6 (20 in Figure 1), with an L_3 centroid at 854.6 eV. The large branching ratio is consistent with the primarily high-spin nature of this complex. Complexes with significant Ni(III) character such as $Ni^{III}DCB$ (13) and $Ni^{III}(cyclam)Cl_2(ClO_4)$ (17) had centroids at 854.3 and 854.5, respectively—well separated from the Ni(II) region. These samples also had lower branching ratios than K_3NiF_6 , and they indeed turn out to be low-spin Ni(III) complexes.

Some formally Ni(III) complexes have spectra quite similar to low-spin Ni(II). For example, the L_3 centroid for $[Ni^{III}pdtc_2]^-$ (15) falls at 854.0 eV, close to low spin Ni(II) complexes with strong ligand fields, such as $[Ph_4P]_2Ni^{II}mac^+$ (26) at 853.8 eV. This indicates that a significant fraction of the positive charge is delocalized onto the ligand, yielding more Ni(II) L^+ character. The potential for ligand oxidation in formally Ni(III) complexes was pointed out as early as 1965 by Stiefel and co-workers.⁵⁸ Finally, for completeness, we include an ionic Ni(IV) complex in our correlation— $KNi^{IV}(IO_6)$ (27). With an L_3 centroid at 855.6 eV, this complex represents the most oxidized form of Ni that we have encountered.

Modified Sample Handling. The fluorescence-detected soft X-ray experiment employs high vacuum conditions around the sample, and there is always a concern that the sample integrity is damaged by exposure to vacuum. We therefore devised a new sample apparatus that allows characterization of the film in situ and keeps a controlled atmosphere above the sample until cool-down is complete. A photograph of this device is included with an exploded sketch in Figure 2. The device consists of a sapphire plate, which mounts inside a threaded, gold-plated

(53) Grush, M. M.; Chen, J.; Stemmler, T. L.; George, S. J.; Penner-Hahn, J. E.; Christou, G.; Cramer, S. P. *J. Am. Chem. Soc.* **1996**, *118*, 8, 65–69.

(54) Peng, G.; van Elp, J.; Jang, H.; Que, L.; Armstrong, W. H.; Cramer, S. P. *J. Am. Chem. Soc.* **1995**, *117*, 2515–2519.

(55) Thole, B. T.; van der Laan, G. *Phys. Rev. B* **1988**, *38*, 3158–3171.

(56) Stöhr, J. *J. Electron Spectrosc. Relat. Phenom.* **1995**, *75*, 253–272.

(57) Peisach, J.; Blumberg, W. E. *Arch. Biochem. Biophys.* **1974**, *165*, 691–708.

(58) Stiefel, E. I.; Waters, J. H.; Billig, E.; Gray, H. B. *J. Am. Chem. Soc.* **1965**, *87*, 3016–3017.

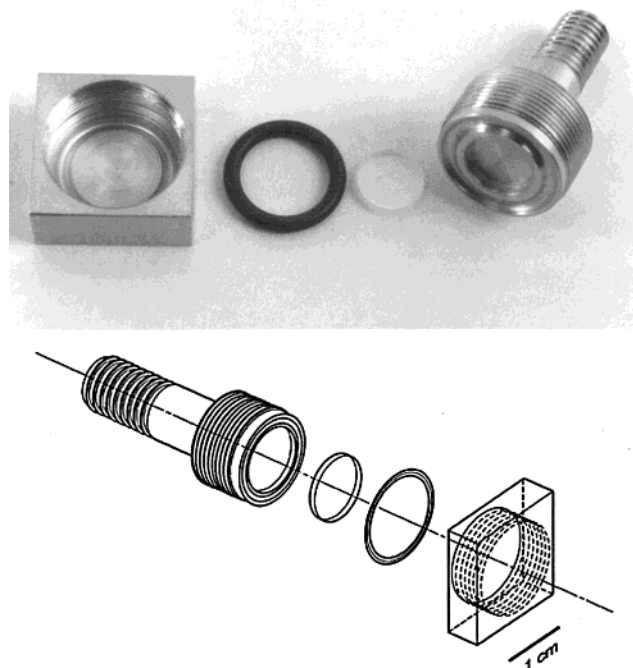


Figure 2. Top—Photograph of the capped sample cell for biological soft X-ray spectroscopy. Bottom—Exploded sketch of the cell assembly.

copper base, which is in turn sealed with an O-ring and a threaded cap. The sample is only exposed to vacuum once the base is attached to the coldfinger and the temperature is close to 20 K. Since the vapor pressure of water is negligible at 20 K, sample lyophilization is no longer a concern. Details concerning the use of this cell are reported in the Experimental Section.

Ct-CODH EPR. To confirm that the enzyme metal clusters in our samples have properties similar to those observed in frozen solutions, we recorded EPR spectra of the films. The EPR spectrum of the “as-isolated” film before L-edge analysis (Figure 3) is dominated by the $g_{av} = 1.82$ EPR signal (features at 2.01, 1.80, and 1.64) that arises from the C-cluster in the partially reduced C_{red1} state.^{13,28} Small amounts of the $g_{av} = 1.86$ EPR signal (from the C_{red2} state of the C-cluster) and the $g = 1.94$ signal (from the B_{red} state of the B-cluster) are also observed. No signal is apparent from the A-cluster; it appears that the composition under these conditions is primarily $A_{ox}:B_{ox}:C_{red1}$.

The CO-treated film before L-edge analysis exhibits a strong B_{red} signal (features at $g = 2.04, 1.94,$ and 1.90) and a mixture of C_{red1} and C_{red2} signals. In fact, it is quite similar to spectra reported by Anderson and Lindahl for Ct-CODH during the early phases of dithionite reduction.²⁸ The NiFeC signal should occur at g -values of 2.08 and 2.028.⁵⁹ However, we note that a $P_{1/2}$ of 0.2 mW at 16 K was reported for the NiFeC signal from *Methanosarcina thermophila* CODH,⁶⁰ hence any NiFeC signal from our sample was saturated. Although the NiFeC signal is not evident under the conditions employed, in parallel experiments on CO-treated films, $10 \pm 5\%$ of the total Ni was converted to the NiFeC form. The only reductant used in the

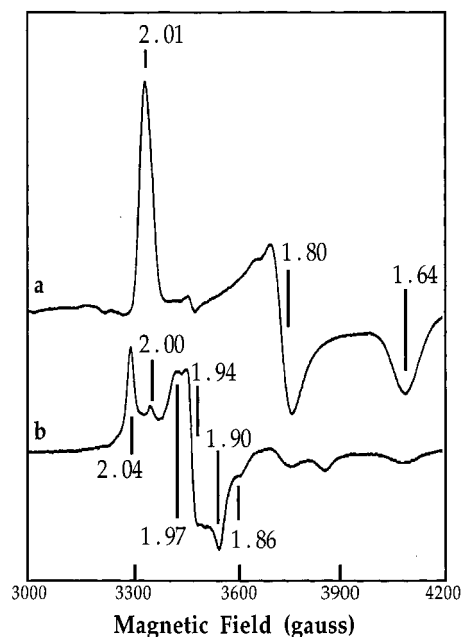


Figure 3. EPR spectra of CODH samples after drying on the silicon wafer, before L-edge analysis. Top to bottom: (a) as-isolated Ct-CODH; (b) CO-treated CODH. EPR conditions: temperature, 10 K; power, 40 mW; modulation amplitude, 12 G; frequency, 9.451 GHz; gain, 2000.

sample preparation was CO, and it clearly changed the redox status of the enzyme.

We were not able to obtain useful EPR spectra for samples after data collection. The enzyme films tend to fall off the support during removal from the vacuum chamber, and the intensities from the remaining fragments are very weak. Furthermore, the trapped radicals that are produced during data collection at 20 K are free to migrate and cause damage when the films are removed from the chamber. Since the L-edge spectra are reproducible and do not change during data collection, we assume that they probe the films in the same form as the “before” EPR spectra.

CODH L-Edges. The L-edges of Ct-CODH under native and CO-treated conditions, recorded with and without the capped cell assembly, are compared with reduced and oxidized Rr-CODH spectra in Figure 4. The native Ct-CODH spectrum has a centroid at 853.7 eV and a branching ratio of 0.68. This falls within the low-spin Ni(II) region of the correlation diagram (Figures 1 and 4). The L_3 spectrum of the CO-treated Ct-CODH sample shows additional absorption intensity at low-energy compared to the as-isolated enzyme; the centroid shifts to 853.2 eV. There is also an increase in branching ratio from 0.68 to 0.70. The “dithionite-reduced” Rr-CODH spectrum has an even higher branching ratio (0.71); the edge is relatively broad with a centroid at 853.6 eV. Finally, indigo carmine oxidation lowers the branching ratio to 0.69 and raises the centroid to 853.9 eV.

Ct-CODH Analysis. From its position in the correlation diagram (Figure 4), we would expect the “as-isolated” Ct-CODH spectrum to resemble those for low-spin Ni(II) complexes. This is indeed the case, and a reasonable simulation is obtained without invoking other types of Ni (Figure 5). If a second high-spin Ni(II) component is added anyway, we estimate that it constitutes $\sim 10\%$ of the total Ni. A low-spin Ni(II) assignment is not unexpected for the 50% of the Ni in the A-cluster, since the K X-ray absorption edge suggests a distorted square planar $Ni^{26,27}$ and such complexes are generally low-spin. The EXAFS data indicating 2.19 (2.18) Å Ni–S and 1.89 (1.82) Å Ni–N/O

(59) Ragsdale, S. W.; Wood, H. G.; Morton, T. A.; Ljungdahl, L. G.; DerVartanian, D. V. In *The Bioinorganic Chemistry of Nickel*; Lancaster, J. R., Ed.; VCH Publishers: New York, 1988; pp 311–332.

(60) Lu, W.-P.; Jablonski, P. E.; Rasche, M.; Ferry, J. G.; Ragsdale, S. W. *J. Biol. Chem.* **1994**, *269*, 9736–9742.

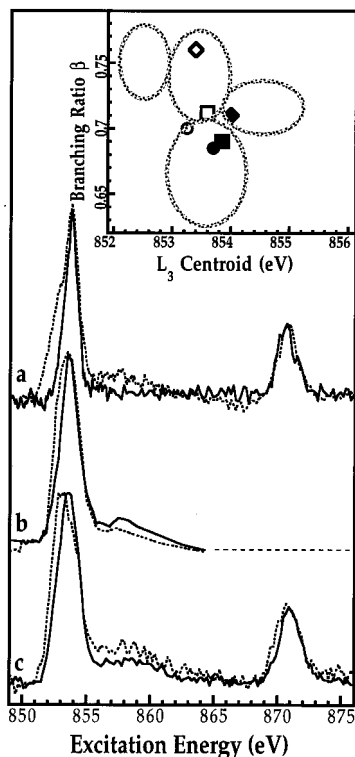


Figure 4. L-edge spectra for all of the CODH samples. Top to bottom: (a) bare samples of native Ct-CODH (—) vs CO-treated Ct-CODH (---); (b) native Ct-CODH (—) vs CO-treated Ct-CODH (---) using capped samples; (c) Rr-CODH in dithionite reduced (---) and indigo carmine oxidized (—) forms. Inset—location of enzyme spectra on the correlation diagram: (a) native Ct-CODH, (b) CO-treated Ct-CODH, (c) dithionite reduced Rr-CODH, and (d) indigo carmine oxidized Rr-CODH. Also for comparison: (e) H₂-reduced (form R) *D. gigas* hydrogenase and (f) as-isolated (form A) *D. gigas* hydrogenase.

distances for the α -subunit or intact protein, respectively, are also typical of low-spin Ni(II).^{27,61} The remaining 50% of the Ni is in the C-cluster, which, in the coupling model of Hu and co-workers,¹³ is proposed to be high-spin Ni(II) in the C_{red1} form. However, the authors note that the C_{red1} fraction only integrates to between 0.1 and 0.6 spin/mol.¹³ It appears that the bulk of the C-cluster must also contain low-spin Ni under our conditions, but it may be in a form or forms distinct from C_{red1}.

The spectral changes upon CO treatment of Ct-CODH are consistent with reduction of a fraction of nickel in Ct-CODH to Ni(I). However, they could also be associated with partially converting low-spin to high-spin Ni(II). We tested these alternatives by fitting the spectrum of CO-treated Ct-CODH with a combination of Ni(I) and Ni(II) model compound spectra, as well as with a combination of high spin and low spin Ni(II) (Figure 5). The best fit uses a mix of Ni(I) and low-spin Ni(II) (Figure 5). However, with the quality of the current data, we cannot rule out a mix of high-spin and low-spin Ni(II) or even a mixture of Ni(I) and both types of Ni(II).

The sum rule for integrated L-edge intensities allows us to quantitatively interpret these fits.³² Because Ni(I) has fewer *d*-shell vacancies than Ni(II), the integrated L_{2,3}-edge (2p → 3d) intensity for Ni(I) is lower. In the language of UV-visible spectroscopy, the “oscillator strength” for Ni(I) L_{2,3}-edges is only about half of that for Ni(II), and a given area for a Ni(I) component represents twice the amount of Ni as does the same area for Ni(II). If the CO-treated spectrum is simulated as Ni(I) plus low-spin Ni(II), the relative intensities of the two

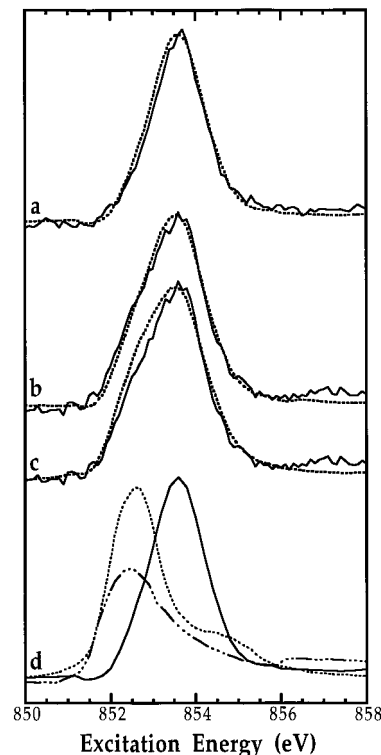


Figure 5. Simulations of Ct-CODH L-edge spectra. Top to bottom: (a) L₃-edge of as-isolated Ct-CODH (—) compared to pure low-spin Ni(II) (---); (b) CO-treated Ct-CODH (—) compared to a simulation (---) using 40% Ni(I) and 60% low-spin Ni(II); (c) CO-treated Ct-CODH (—) compared to a simulation (---) using 30% high-spin Ni(II) and 70% low-spin Ni(II); (d) spectra of the model compounds used for the fits: Ni(I), (Ni^I“S₄”) (— · — · —); high-spin Ni(II), (Ni(DAPA)-(SePh)₂) (---); low-spin Ni(II), (Ni^{II}“S₄”) (—). Additional model compound details are included as supporting information.

components indicate that Ni(I) represents about 30–50% of the total Ni. If the spectral change were due to formation of high-spin Ni(II), then the fits suggest ~20–30% high-spin Ni.

Since only ~15% of the total Ct-CODH Ni forms an EPR-active CO complex, the amount of predicted Ni(I) is actually more than expected on the basis of the Ni–Fe–C signal alone. One possibility is that some of the C-cluster Ni is also partially reduced under these conditions. However, the results can also be explained by an increase in the fraction of high-spin Ni(II) after CO treatment, and further work is needed with more homogeneous systems to settle these issues.

Rr-CODH Simulations. The C-cluster of CODH is more readily studied in the *R. rubrum* enzyme, where it is the only Ni-containing center. Simulations of the L-edge spectra of dithionite-reduced Rr-CODH and indigo-carmin oxidized Rr-CODH are shown in Figure 6. The energy of the L₃ centroid of the dithionite-reduced sample (853.6 eV) falls in the Ni(II) region, while the branching ratio (0.71) is near the border between typical high-spin and low-spin values. The dithionite-reduced spectrum is also broader than model compound spectra with a single Ni species.

The simplest explanation of the dithionite-reduced Rr-CODH L-edge data is that the samples contain both low-spin and high-spin Ni(II) under our conditions. It can be simulated by a mixture of 40% low-spin and 60% high-spin Ni(II) components (Figure 6). EPR and Mössbauer spectroscopy have already provided ample evidence for C-cluster heterogeneity. For example, Hu and co-workers found that in dithionite-reduced Rr-CODH, 50–70% of the C-clusters is in the C_{S=3/2} state, while about 40% is

(61) Ralston, C. Y. Ph.D. Thesis, University of California, Davis, 1997.

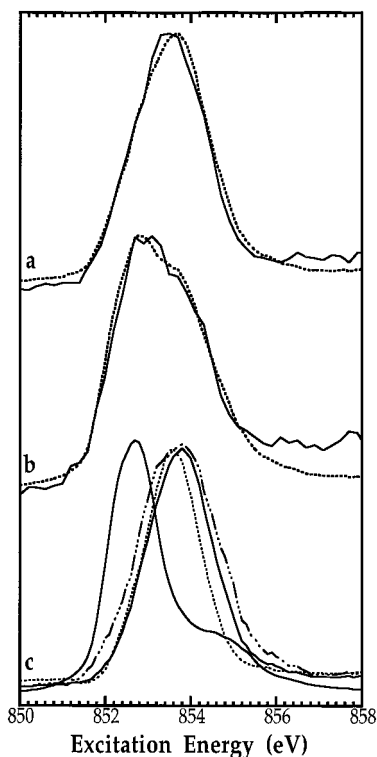


Figure 6. Simulations of Rr-CODH L-edge spectra. Top to bottom: (a) dithionite-reduced Rr-CODH (—) and fit (---) using 40% low-spin Ni(II) and 60% high-spin Ni(II); (b) indigo carmine oxidized enzyme (—) and (---) fit using 85% low-spin Ni(II) and 15% high-spin Ni(II); (c) spectra of the model compounds used for the fits: high-spin Ni(II), Ni(DAPA)(SePh)₂ (—); low-spin Ni(II), Ni^{III}'DCB'' (— · —); low-spin Ni(II), Ni^{III}'S₄' (· · ·); low-spin Ni(III), [Ni^{III}(pdte)₂]⁻ (— · · ·).

in the C_{red2} state.¹³ Furthermore, they note that the samples have to be frozen within 1–2 min after reduction for the C_{red2} signal to be obtained. In partially reduced samples poised at –300 mV, the C_{red1} EPR signal integrated to ~0.65 spin (relative to the B_{red} signal).¹³ Unfortunately, none of the magnetic resonance data addresses the status of the Ni site, since ⁶¹Ni ENDOR signals are not observed for C_{red1} or C_{red2}.⁶²

The Ni L-edge centroid of the indigo carmine oxidized Rr-CODH sample (Figure 6) is shifted to higher energy (853.9 eV) from the dithionite-reduced spectrum. This result was reproduced in three individual experiments. There are two alternative explanations for this observation. In one scenario, addition of indigo carmine oxidizes the Ni(II) to a covalent Ni(III) species. As shown in Figure 6, the L-edge spectrum of oxidized Rr-CODH does resemble that of the covalent Ni(III) complex [Ni(pdte)]⁻.⁶³ However, there is no EPR evidence for a Ni(III) species.

A more conventional explanation for the L-edge change is a spin-state shift caused by structural changes in the Ni environment. The oxidized Rr-CODH spectrum can be fit by a mixture of 15% high-spin Ni(II) and 85% low-spin Ni(II) (Figure 6). Small geometry changes and/or ligand changes can result in high-spin to low-spin conversions at Ni sites.⁶⁴ In Rr-CODH, such a change might involve the ligand proposed to bridge between Ni and the FCII Fe of the Fe₄S₄ cluster.¹³ Even if redox activity is localized at the Fe site, a change in the Ni–Fe bridge

(62) DeRose, V. J.; Telser, J.; Anderson, M. E.; Lindahl, P. A.; Hoffman, B. M. *J. Am. Chem. Soc.* **1998**, *120*, 8767–8776.

(63) Krüger, H.-J.; Holm, R. H. *Inorg. Chem.* **1987**, *26*, 3645–3647.

(64) Coyle, C. L.; Stiefel, E. I. In *The Bioinorganic Chemistry of Nickel*; Lancaster, J. R., Jr., Ed.; VCH Publishers: New York, 1988; pp 1–28.

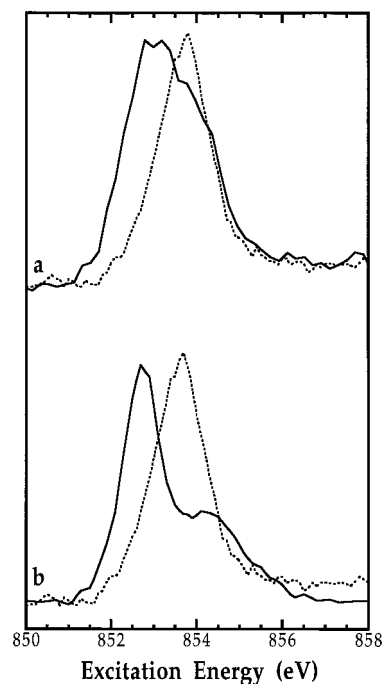


Figure 7. Comparison of L-edge spectra for predominantly high-spin vs low-spin Ni enzyme samples. Top to bottom: (a) as-isolated Ct-CODH (---) compared to dithionite-reduced Rr-CODH (—); (b) as-isolated Ct-CODH (---) compared to H₂-reduced *D. gigas* hydrogenase (—).

could induce a Ni spin-state change. For example, one possibility is that oxidation of the associated Fe₄S₄ cluster breaks the Ni–X–Fe bridge, resulting in loss of a Ni axial ligand and conversion to a more square planar geometry. This would explain the shift to primarily low-spin Ni(II). Furthermore, if the lost ligand were a cysteine thiolate, the low-spin Ni would be in a less covalent environment and would have a higher energy L₃ centroid.

Overall, this study has shown that both CODH A- and C-clusters often utilize the low-spin Ni(II) state. This is in sharp contrast with our Ni–Fe hydrogenase results, where the Ni site is most frequently in the high-spin Ni(II) form. The dramatic difference in CODH and H₂ase spectra is illustrated in Figure 7, as well as in the inset of Figure 4.

Conclusions

We (and others) have found that L-edge XAS is able to distinguish between different spin and oxidation states of Ni compounds. We have used this capability to characterize two CODH proteins, both of which can contain heterogeneous nickel populations. Low-spin Ni(II) was found to be the dominant Ni component in as-isolated Ct-CODH samples. This is in contrast with Ni hydrogenases, where reduced samples contain mostly high-spin Ni(II).^{41,43,65} CO-treatment of Ct-CODH elicited a new form of Ni, which is either Ni(I), high-spin Ni(II), or a mixture of both species. Dithionite-reduced Rr-CODH was also found to be heterogeneous and is best modeled as a mixture of low-spin and high-spin Ni(II). Finally, we found that indigo carmine oxidation of Rr-CODH produced a Ni L-edge spectrum similar to almost homogeneous low-spin Ni(II) or very covalent Ni(III).

The experimental sensitivity of L-edge spectroscopy is now adequate for obtaining spectra on protein films. The introduction of more powerful undulator beamlines⁶⁶ and higher resolution

(65) Ralston, C.; Chen, J.; Peng, G.; George, S. J.; van Elp, J.; Cramer, S. P. *Physica B* **1995**, *209*, 203–208.

detectors⁶⁷ will make measurements possible on dilute frozen solutions. L-edges can reveal information about electronic structure that is difficult or impossible to obtain by other

(66) Young, A. T.; Martynov, V.; Padmore, H. *J. Electron Spectrosc. Relat. Phenom.* **1999**, *103*, 885–889.

(67) Friedrich, S.; Mears, C. A.; Nideröst, B.; Hiller, L. J.; Frank, M.; Labov, S. E.; Barfknecht, A. T.; Cramer, S. P. *Microsc. Microanal.* **1998**, *4*, 616–621.

(68) Lovecchio, F. V.; Gore, E. S.; Busch, D. H. *J. Am. Chem. Soc.* **1974**, *96*, 3109–3118.

(69) Szalda, D. J.; Fujita, E.; Sanzenbacher, R.; Paulus, H.; Elias, H. *Inorg. Chem.* **1994**, *33*, 5855–5863.

(70) Baidya, N.; Olmstead, M. M.; Mascharak, P. K. *Inorg. Chem.* **1991**, *30*, 929–937.

(71) Marganian, C. A.; Vazir, H.; Baidya, N.; Olmstead, M. M.; Mascharak, P. K. *J. Am. Chem. Soc.* **1995**, *117*, 1584–1594.

(72) Barefield, E. K.; Wagner, F.; Flerlinger, A. W.; Dahl, A. R. *Inorg. Synth.* **1976**, *16*, 220–225.

(73) Ito, T.; Sugimoto, M.; Toriumi, K.; Ito, H. *Chem. Lett.* **1981**, 1477–1478.

(74) Kruger, H.-J.; Peng, G.; Holm, R. H. *Inorg. Chem.* **1991**, *30*, 734–742.

(75) Collins, T. J.; Kostka, K. L.; Uffelman, E. S.; Weinberger, T. L. *Inorg. Chem.* **1991**, *30*, 4204–4210.

(76) Shoner, S. C.; Olmstead, M. M.; Kovacs, J. A. *Inorg. Chem.* **1994**, *33*, 7–8.

(77) Cha, M. Y.; Catlin, C. L.; Critchlow, S. C.; Kovacs, J. A. *Inorg. Chem.* **1993**, *32*, 5868–5877.

(78) Stein, L.; Neil, J. M.; Alms, G. R. *Inorg. Chem.* **1969**, *8*, 2472–2476.

methods. As the experiment becomes easier and more accessible, soft X-ray spectroscopy should become a valuable tool for the study of metals in biology.

Acknowledgment. We gratefully acknowledge the following people for supplying Ni model compounds used in this study: Dr. E. Fujita, Prof. J. A. Kovacs, Dr. M. Woome and Prof. T. J. Collins, Dr. C. A. Marganian and Prof. P. K. Mascharak, Prof. M. J. Maroney, Prof. M. W. W. Adams, and Mr. J. Allman. This work was supported by the National Institutes of Health Grants GM-44380 (S.P.C.) and GM-39451 (S.W.R), Department of Energy Grants ER20053 (S.W.R) and DE-FG02-87ER13691 (P.W.L.), and the DOE Office of Biological and Environmental Research (S.P.C.).

Supporting Information Available: Table 1 of model compound data used to generate Figure 1 (PDF). This material is available free of charge via the Internet at <http://pubs.acs.org>.

JA0009469

(79) Ge, P. H.; Riordan, C. G.; Yap, G. P. A.; Rheingold, A. L. *Inorg. Chem.* **1996**, *35*, 5408–5409.

(80) Brooker, S.; Croucher, P. D.; Roxburgh, F. M. *J. Chem. Soc., Dalton* **1996**, 3031–3037.

(81) Mansour, A. N.; Melendres, C. A. *Physica B* **1995**, *209*, 583–584.

(82) Colpas, G. J.; Kumer, M.; Day, R. O.; Maroney, M. J. *Inorg. Chem.* **1990**, *29*, 4779–4788.